

1 Direct *In-Situ* Mass Specific Absorption Spectra of
2 Biomass Burning Particles Generated from
3 Smoldering Hard and Softwoods

4 *James G. Radney[†], Rian You^{†‡}, Michael R. Zachariah^{†‡} and Christopher D. Zangmeister^{†*}*

5
6 [†]Material Measurement Laboratory, National Institute of Standards and Technology,
7 Gaithersburg, Maryland 20899.

8
9 [‡]Department of Chemistry and Biochemistry, University of Maryland, College Park, Maryland
10 20742.

11
12 **ABSTRACT**

13 Particles from smoldering biomass burning (BB) represent a major source of carbonaceous aerosol
14 in the terrestrial atmosphere. In this study, mass specific absorption spectra of laboratory-generated
15 smoldering wood particles (SWP) from 3 hardwood and 3 softwood species were measured *in-*
16 *situ*. Absorption data spanning from $\lambda = 500$ nm to 840 nm were collected using a photoacoustic
17 spectrometer coupled to a supercontinuum laser with a tunable wavelength and bandwidth filter.
18 SWP were size- (electrical mobility) and mass-selected prior to optical characterization allowing
19 data to be reported as mass-specific absorption cross sections (*MAC*). The median measured *MAC*
20 at $\lambda = 660$ nm for smoldering oak particles was $1.1 (0.57/1.8) \times 10^{-2} \text{ m}^2 \text{ g}^{-1}$ spanning from 83
21 femtograms (fg) to 517 fg ($500 \text{ nm} \leq \text{mobility diameter} \leq 950 \text{ nm}$), *MAC* values in parenthesis are

22 the 16th and 84th percentiles of the measured data (i.e. 1σ). The collection of all six wood species
23 (Oak, Hickory, Mesquite, Western redcedar, Baldcypress and Blue spruce) had median *MAC*
24 values ranging from $1.4 \times 10^{-2} \text{ m}^2 \text{ g}^{-1}$ to $7.9 \times 10^{-2} \text{ m}^2 \text{ g}^{-1}$ at $\lambda = 550 \text{ nm}$ with absorption Ångström
25 exponents (*AAE*) between 3.5 and 6.2. Oak, Western redcedar and Blue spruce possessed
26 statistically similar ($p > 0.05$) spectra while the spectra of Hickory, Mesquite and Baldcypress
27 were distinct ($p < 0.01$) as calculated from a point-by-point analysis using the Wilcoxon rank-sum
28 test.

29 INTRODUCTION

30 Biomass burning (BB) is estimated to contribute $> 35 \%$ to the global emission of carbonaceous
31 aerosol by mass.¹ The major particle-phase constituents generated from BB combustion can be
32 optically categorized into 3 broad groups: black carbon (BC), absorbing organic carbon (brown
33 carbon, BrC) and non-absorbing organic carbon (OC).² The mix of BC, BrC and OC emitted
34 depends upon conditions with BC preferentially formed during flaming and BrC and OC during
35 smoldering combustion.^{3,4}

36 The net positive radiative forcing^{5,6} of BC is second only to CO_2 , due to its strong, and nearly
37 wavelength independent, absorption and low single scattering albedo across the visible spectrum
38 ($\lambda = 400 \text{ nm}$ to 700 nm).⁷ BrC absorption is much lower than BC and is strongly wavelength
39 dependent, being weak or negligible in the near-IR and significantly increasing towards the UV.⁸
40 The BrC wavelength dependence introduces large uncertainties into radiative forcing calculations⁴
41 with predictions of BrC's climate impact ranging from net neutral⁹ to net positive.^{10,11} One input
42 into climate models are the BC and BrC mass-specific absorption cross sections (*MAC*, $\text{m}^2 \text{ g}^{-1}$).
43 Depending on the instrumentation and method used, *MAC* can take a variety of forms

$$44 \quad MAC = \frac{\alpha_{abs}}{Nm_p} = \frac{C_{abs}}{m_p} = \frac{\alpha_{abs}}{\rho V} = \frac{\alpha_{abs}}{M} \quad (1)$$

45 where α_{abs} (m^{-1}), N (m^{-3}), m_p (g), C_{abs} (m^2), ρ (kg m^{-3}), V (m^3 of aerosol per m^3 of air), and M (g of
 46 aerosol per m^3 of air) are the aerosol absorption coefficient, the aerosol number density, the
 47 average particle mass, the absorption cross section ($C_{Abs} = \alpha_{abs}/N$), the average particle mass
 48 density, the volume fraction of aerosol particles and the mass concentration of aerosol particles (M
 49 $= Nm_p = \rho V$), respectively. The corresponding units for each parameter are shown in parenthesis.
 50 The wavelength dependent absorption is commonly described by the absorption Ångström
 51 exponent (AAE)

$$52 \quad MAC_{\lambda} = MAC_{\lambda_0} \left(\frac{\lambda}{\lambda_0} \right)^{-AAE} \quad (2)$$

53 where λ and λ_0 are an arbitrary wavelength in the spectrum and a reference wavelength,
 54 respectively. In this study, Eq. 2 has been defined by MAC , although C_{abs} or α_{abs} could also be
 55 used. Ångström exponents were originally used to describe the wavelength dependence of
 56 extinction for high albedo materials,¹² but have also been used to describe the wavelength
 57 dependence of particle absorption even though a single AAE value may not accurately describe the
 58 entire spectrum; see Moosmüller, et. al (2011)¹³ and references therein.

59 BB aerosol optical properties can be measured in the field during uncontrolled¹⁴⁻¹⁶ or prescribed
 60 fires.^{17,18} Laboratory measurements use more controlled combustion^{4,19-25} or pyrolysis²⁶ conditions
 61 with known fuel types and quantities. BB MAC have been indirectly measured using two primary
 62 instrumental platforms: filters and photoacoustic spectroscopy (PAS). Filter measurements collect
 63 particles and low-volatility OC components and absorption is inferred either through changes in
 64 filter attenuation^{24,27} (a surrogate for absorption) or extraction by solvents followed by subsequent
 65 measurement of the solution absorption spectrum with relatively high spectral resolution (< 20
 66 nm).^{16,26,28} Filter-based measurements cannot completely capture aerosol MAC , as the method is

67 not quantitative on a per mass basis due to challenges in measuring deposited particle mass, filter
68 artifacts (multiple scattering, shadowing, evaporative loss, adsorptive gain, etc.), solvent extraction
69 efficiencies and the assumption that the absorption spectrum of the collected material is unaffected
70 by solvation.

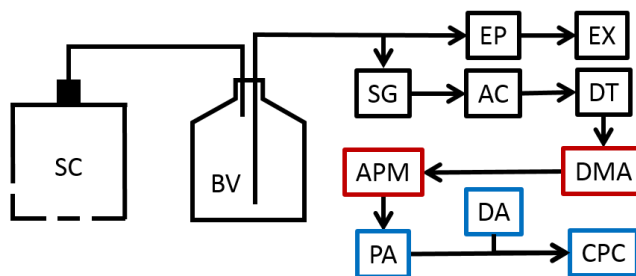
71 The second platform uses PAS to measure absorption coefficients and the average *MAC* for an
72 entire population is determined indirectly using the third or fourth forms of Eq. 1
73 ($MAC = \frac{\alpha_{abs}}{\rho V} = \frac{\alpha_{abs}}{M}$). Average density is either assumed or calculated from measured chemical
74 composition mass fractions.^{22,23} Volume distributions are inferred from the measured size
75 distributions (assuming spherical particles). Mass concentrations are determined
76 gravimetrically,^{14,19-21,25} using an aerosol mass spectrometer²⁹ or a laser induced incandescence
77 instrument (elemental carbon only).¹⁸ Each of the measured quantities requires separate
78 instrumentation operated simultaneously and in parallel. This method is highly sensitive to the
79 accuracy of ρ , V and M and any error in data collection or fitting amplifies *MAC* uncertainty
80 without consideration to inherent particle variability.^{19,22,23} Further, *MAC* values are typically
81 reported at a single wavelength. When multiple wavelengths are available, *AAEs* are calculated
82 from pairwise fits of the PAS data or from multi-wavelength filter attenuation data in conjunction
83 with PAS data to correct for filter biases.³⁰ Method uncertainties have led to conflicting
84 interpretations on the influence of combustion conditions and/or fuel type on BB particle
85 absorption.^{22,31}

86 To ascertain the influence of wood specie on the optical properties of smoldering combustion,
87 three conditions are required: 1) optimally controlled conditions to minimize intra- and inter-
88 experiment variability, 2) low measurement uncertainties relative to the intra-experiment and
89 wood specie variation and 3) quantification of experimental uncertainties (Type A and Type B) to

90 isolate inter-specie variation from method uncertainties. The current investigation measures the
 91 *MAC* of smoldering wood particles (SWP) under well-controlled conditions across a broad
 92 wavelength range for 6 fuel types using photoacoustic spectroscopy; however, unlike previous
 93 investigations, *MAC* was determined using the first form of Eq. 1 ($MAC = \frac{\alpha_{abs}}{Nm_p}$); notably, α_{abs} , N
 94 and m_p are all directly measured quantities.³² Absorption data was collected for mobility- and
 95 mass-selected particles at 8 wavelengths between $\lambda = 500$ nm and 840 nm using a photoacoustic
 96 spectrometer (PA) and step-scanning a supercontinuum laser coupled to a tunable wavelength and
 97 bandwidth filter. Wood specie variation was larger than quantified method uncertainty and inter-
 98 experiment variability facilitating determination of wood specie influence on *MAC* spectra on a
 99 statistical basis.

100 MATERIALS AND METHODS

101 A schematic of the experimental setup is shown in Figure 1 which includes components to
 102 generate and condition, size- and mass-select (differential mobility analyzer, DMA, and aerosol
 103 particle mass analyzer, APM, respectively) and measure the absorption spectra (photoacoustic
 104 spectrometer, PA) and number density (condensation particle counter, CPC) of the SWP; these
 105 components are shown with black, red and blue outlines, respectively.



106
 107 **Figure 1:** Experiment schematic. Black: aerosol generation and conditioning. Red: size and mass
 108 selection. Blue: spectroscopic characterization. Abbreviations: smoldering chamber (SC), 20 L

109 buffer volume (BV), ejector pump (EP), exhaust (EX), silica gel diffusion dryer (SG), activated
110 carbon diffusion dryer (AC), drying tube (DT), differential mobility analyzer (DMA), aerosol
111 particle mass analyzer (APM), photoacoustic spectrometer (PA), dilution air (DA), condensation
112 particle counter (CPC).

113 **SWP generation.** Six wood species were investigated including hardwoods consisting of Oak
114 (mixture of *Quercus falcata* and *Quercus alba*), Hickory (mixture of *Carya ovata* and *Carya*
115 *texana*) and Mesquite (*Prosopis juliflora*) and softwoods of Western redcedar (*Thuja plicata*),
116 Baldcypress (*Taxodium distichum*) and Blue spruce (*Picea pungens*). The Hickory, Mesquite,
117 Western redcedar and Baldcypress were sourced from commercially available wood chips. Oak
118 chips and Blue spruce twigs were collected from the grounds of the National Institute of Standards
119 and Technology (NIST) located in Gaithersburg, Maryland USA. All samples were pre-treated at
120 100 °C overnight to remove bulk water.³³

121 Smoldering was initiated using in an in-house built combustor contained within a laboratory
122 fume hood. The combustor consisted of a 0.95 L (1 qt) stainless steel can 10.8 cm tall and 12.38
123 cm in diameter with seven 0.556 cm diameter air holes (three on side wall and four at bottom
124 center) to supply air. An exit port in the lid was fashioned from a 1.27 cm (1/2 in) NPT galvanized
125 steel flange connected to a 1.27 cm (1/2 in) NPT galvanized steel tube and 0.952 cm (3/8 in) stainless
126 steel tube. Using a downstream ejector pump, a constant and controlled amount of air ($\approx 10 \text{ L min}^{-1}$)
127 was pulled into the smoldering chamber via the air holes, over the smoldering wood, through
128 the exit port and delivered to a 20 L glass carboy buffer volume; nominal carboy residence time
129 was 2 minutes. All transfer lines consisted of conductive silicone tubing or stainless steel to
130 minimize particle loss and deposition. For each run, $\approx 100 \text{ g}$ of fuel was used. The fuel was ignited
131 at the bottom of the smoldering chamber using a propane torch. SWP were observed in the buffer

132 volume nearly immediately upon application of the heat source to the wood sample. Following the
133 airflow recommendations of Ohlemiller,³⁴ stable smoldering was able to be maintained for up to
134 60 min. On rare occasions, flaming was visible in the combustor and limited to small parts of the
135 sample, cessation was rapid due to limited O₂ (air flow was constant) resulting in continuation of
136 smoldering.

137 SWP were sampled prior to the ejector pump at a flowrate of 0.5 L min⁻¹. Multiple steps were
138 used to limit the impact of residual combustion gases and condensable water vapor and to maintain
139 a constant relative humidity over the course of a single smoldering experiment. Residual
140 combustion gases were removed by passing the particles through a diffusion dryer filled with
141 activated carbon. Water vapor was removed by passing the particles through a diffusion dryer
142 filled with silica gel desiccant and a monotube gas dryer. Silica desiccant was changed prior to
143 each experiment. Under these conditions the relative humidity in the DMA was maintained at <
144 8 %.

145 **Size and mass classification.** SWP were size-selected at a given mobility diameter (D_m) using
146 an electrostatic classifier with long DMA column that was operated with an aerosol flow of 0.5 L
147 min⁻¹ and a sheath flow of 2.5 L min⁻¹. Particles were mass selected using an APM that was
148 operated either in scanning mode for the determination of the average mass of particles with $q \geq$
149 $+1$ – see Radney and Zangmeister (2016)³⁵ – or static mode to measure absorption spectra where
150 the APM was set to the average mass of the $q = +1$ distribution.

151 This combination of DMA-APM also enables determination of the effective density (ρ_{eff})^{36,37}
152 from

153
$$\rho_{eff} = \frac{6m_p}{\pi D_m^3} \quad (3)$$

154 where m_p is the average mass of $q = +1$ charged particles determined from the mass distribution
155 measured by the APM.

156 **Absorption measurements.** The absorption coefficients of size- and mass-selected SWP were
157 measured at eight wavelengths spanning from $\lambda = 500$ nm to 840 using a PA with a supercontinuum
158 laser and tunable wavelength and bandwidth filter. The reader is directed to Radney and
159 Zangmeister (2015)³⁸ for a detailed description on the determination of α_{abs} using the
160 supercontinuum PA. Similar to this previous investigation, wavelength regions were randomized
161 at the beginning of each experiment to reduce systematic bias as a result of collection order.

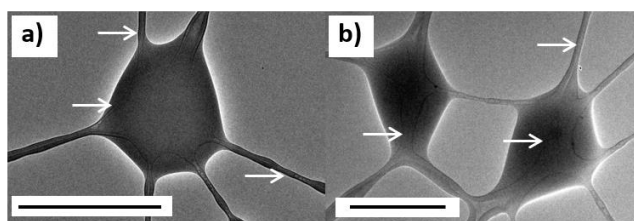
162 *AAEs* were calculated by fitting median *MAC* values to Eq. 2 with $\lambda_0 = 550$ nm; reported
163 uncertainties represent fits of the 16th and 84th percentile data (see Supporting Information for a
164 full discussion of data analysis). To test for spectral similarity, the Wilcox rank-sum test was
165 performed on a wavelength-by-wavelength basis using post-processed data; uncertainties were
166 asymmetric about the median and the number of data points in each spectrum were not equivalent
167 necessitating the use of a non-parametric test. Spectra with > 4 out of 8 data points possessing a
168 statistically significant ($p < 0.01$) difference from all other spectra were considered distinct.

169 **TEM characterization.** Size- and mass-selected SWP were collected on TEM grids (200-mesh
170 copper grids coated with lacey carbon film) using an electrostatic aerosol precipitator at -9.3 kV
171 collection voltage, and an aerosol flow of 0.5 L min⁻¹. TEM images were collected at an
172 accelerating voltage of 200 kV.

173 RESULTS

174 **Particle Characterization.** Low temperature combustion produces primarily liquid particles
175 formed from the condensation of gaseous organic compounds minimizing the formation of BC.²⁷
176 Figure 2 shows TEM images of Oak and Blue spruce SWP at $m_p = 270$ fg ($D_m = 750$ nm) and the

177 white arrows designate selected regions of the underlying TEM grid. No aggregated solid particles
178 (i.e. BC)^{39,40} were observed. Instead, the grids are nearly universally coated by a thin liquid layer
179 with membranes spanning the individual TEM grid fibers suggesting the particles conform to the
180 grid upon impact, similar to previous observations of BB particles⁴¹ (see Supporting Information
181 for additional TEM images). For reference, the scale bars in Figure 2 correspond to 1000 nm and
182 the selected particle mobility diameters were 750 nm. Thus, each image likely contains material
183 from a single particle (Oak, Figure 3a) or a couple of particles (Blue spruce, Figure 3b).



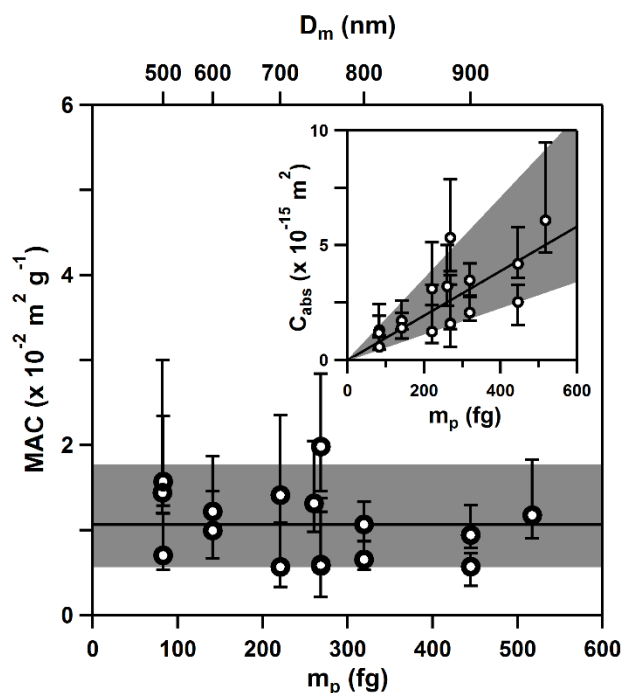
184

185 **Figure 2:** TEM images of collected from a) Oak and b) Blue spruce $m_p = 270$ fg ($D_m = 750$ nm)
186 SWP. Liquid-like material forms coatings on the TEM grid and membranes at grid junctions. Scale
187 bars are 1000 nm. White arrows point towards the underlying TEM grid.

188 **SWP Density Measurements.** Particle densities from SWP were determined for the six wood
189 species under investigation using mass distributions from mobility selected particles.^{32,36,37} Particle
190 densities ranged between 1.31 g cm⁻³ for Blue spruce and Baldcypress up to 1.51 g cm⁻³ for
191 Mesquite, see Table 1. These values are similar to densities derived from mobility and
192 microbalance measurements of organic carbon from BB and densities calculated from
193 compositional analysis of particles collected during flaming combustion from a variety of North
194 American biomass.^{14,22}

195 **Smoldering Wood Absorption.** Wood smoldering produced particles across a broad mass
196 range. Particles were initially mobility classified (D_m) and subsequently mass selected (m_p) prior

197 to entering the PAS, allowing all measurements to be reported on a per mass basis (a SI traceable
198 quantity) versus electrical mobility which is morphology dependent. SWP were first measured at
199 a single wavelength (660 nm) to study particle absorption as a function of m_p , see Figure 3. The
200 *MAC* of oak SWP was $1.1 (0.57/1.8) \times 10^{-2} \text{ m}^2 \text{ g}^{-1}$ at $\lambda = 660 \text{ nm}$ for particles between 83 fg and
201 517 fg ($500 \text{ nm} \leq D_m \leq 950 \text{ nm}$). Each data point represents an independent experiment where the
202 wood sample was replaced and smoldering was initiated. The variability in measured *MAC* is
203 dominated by inter-experiment variability (e.g. sample-to-sample variability) and not intra-
204 experiment variability. The solid black line and shaded area represent the measured median ($1.1 \times$
205 $10^{-2} \text{ m}^2 \text{ g}^{-1}$) and the 16th ($0.57 \times 10^{-2} \text{ m}^2 \text{ g}^{-1}$) and 84th ($1.8 \times 10^{-2} \text{ m}^2 \text{ g}^{-1}$) percentiles (i.e. 1σ),
206 respectively, across all data. The inset of Figure 3 shows C_{abs} as a function of mass, the slope of
207 the linear fit is *MAC* for the range of measured m_p (9.7 ± 1.0) $\times 10^{-3} \text{ m}^2 \text{ g}^{-1}$; uncertainty is 1 standard
208 deviation of the linear fit of C_{abs} vs. m_p without regard to underlying C_{abs} uncertainties.
209 Importantly, within experimental uncertainties, BrC *MAC* is independent of m_p across the
210 measured mass range (i.e. particles are behaving as volume absorbers).⁴² Considering the absolute
211 magnitude of *MAC* measured at $\lambda = 660 \text{ nm}$, the linear relationship of C_{abs} with m_p will hold across
212 the entire range of measured wavelengths (see Supporting Information).

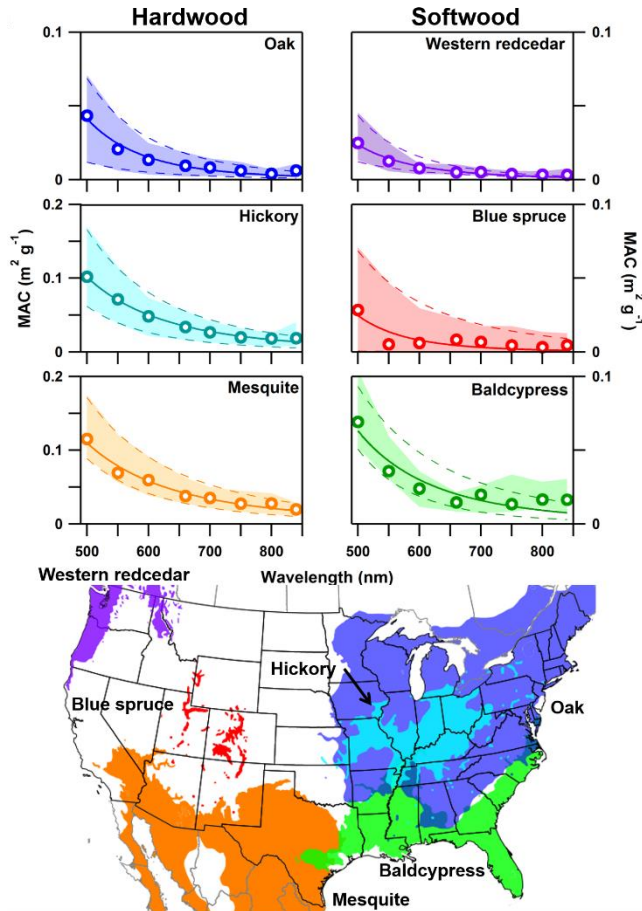


213

214 **Figure 3:** Median *MAC* of oak SWP as a function of particle mass (bottom axis) and mobility
 215 diameter (top axis). Uncertainties in *MAC* represent the 16th and 84th percentiles (i.e. 1σ). Solid
 216 black line and greyed area represent the median *MAC* and uncertainty across all measured data at
 217 all masses, respectively. Inset shows C_{abs} as function of particle mass (m_p). Solid black line
 218 represents fit of data and greyed area represents uncertainty of fit. Slope is *MAC* for the range of
 219 measured m_p .

220 For Oak SWP, C_{abs} at $\lambda = 660$ nm scales linearly with mass thereby demonstrating that only a
 221 single size and mass combination was necessary to determine *MAC* for each wood specie.
 222 Spectroscopic measurements were performed where the largest mass concentration ($D_m = 750$ nm,
 223 $m_p \approx 270$ fg) and hence absorption coefficients were obtained, as shown by Eq. 1: $\alpha_{abs} = M \cdot MAC$.
 224 The measured values of *MAC* were similar enabling the single size and mass combination to be
 225 used for all wood species.

226 Figure 4 shows the *MAC* spectra of mass-selected ($D_m = 750$ nm) SWP for wood six species;
227 data points represent the median measured data collected from between 15 and 70 absorption
228 spectra per smoldering experiment. Shaded regions represent the 16th and 84th percentiles (i.e. 1σ).
229 Solid and dashed lines represent *AAE* fits to the median and 16th and 84th percentiles, respectively;
230 median *MAC* at $\lambda = 550$ nm ($MAC_{\lambda,0}$ in Eq. 2) and *AAE* are shown in Table 1 with percentiles
231 shown in parenthesis. All data was well described using Eq. 2 with the exception of Baldcypress.
232 Eq. 2 is typically only used in discrete pairwise calculations due to a lack of spectral resolution.
233 The presented *in-situ* SWP absorption data have the highest reported spectral resolution to date
234 and all of the measured data was used to fit to the noted power law dependence. However, the
235 spectra may indicate the presence of more complex wavelength dependencies than can be
236 described by a single power law, suggesting that multiple *AAEs* may be required.¹³



237

238 **Figure 4:** Measured *MAC* as a function of wavelength for SWP from six species of wood. Open
 239 circles and shaded areas represent the median *MAC* values and the 16th and 84th percentiles (i.e.
 240 1σ) at each wavelength, respectively; solid and dashed lines represent *AAE* fits to the median and
 241 16th and 84th percentile values, respectively. Wood species distribution is shown on map at
 242 bottom and correspond to the colors of each species absorption spectrum. Map was generated
 243 from level 1 global administrative area basemaps⁴³ overlaid with tree species range maps⁴⁴ using
 244 geographic information systems software.

245 **Table 1:** Measured effective density, median *MAC*, *AAE* and calculated mass % BC, BrC *MAC*
 246 and *AAE*

Species	Effective Density (g cm ⁻³)	Median <i>MAC</i> (x 10 ⁻² m ² g ⁻¹) ^a	<i>AAE</i> ^a	Mass % BC ^b	BrC <i>MAC</i> (x 10 ⁻² m ² g ⁻¹) ^c	BrC <i>AAE</i> ^c
Oak ^d	1.41 (0.04)	2.5 (0.76/4.3)	5.5 (4.8/4.7)	0.09	1.1	11
Hickory ^d	1.44 (0.05)	7.0 (4.0/11)	3.8 (4.0/4.7)	0.4	3.7	7.0
Mesquite ^d	1.51 (0.03)	7.9 (6.0/12)	3.5 (3.5/4.2)	0.4	4.6	7.2
Western redcedar ^e	1.36 (0.03)	1.4 (0.81/2.6)	5.2 (5.6/4.3)	0.07	0.77	10
Blue spruce ^e	1.35 (0.02)	1.4 (0.039/4.7)	6.2 (3.9/3.4)	0.09	0.069	35
Baldcypress ^e	1.35 (0.01)	4.3 (3.0/6.6)	4.1 (3.6/5.5)	0.3	0.90	16

247
248 ^a $\lambda = 550$ nm value calculated from *AAE* fit (Eq. 2) of average values spanning $\lambda = 500$ nm to 840 nm. Values in parenthesis are the values from fits
249 of the 16th and 84th percentile data.

250 ^b Upper bound of BC % mass. Assumes no refractive index matching.

251 ^c $\lambda = 550$ nm value calculated assuming all absorption at $\lambda = 840$ nm is due to BC. See discussion in text.

252 ^d hardwood

253 ^e softwood

254 The measured SWP *MAC* were two orders of magnitude lower than the cited *MAC* of BC^{7,45} with
255 the highest measured median *MAC* = 7.9 (6.0/12) x 10⁻² m² g⁻¹ for Mesquite at $\lambda = 550$ nm; values
256 in parenthesis are the 16th and 84th percentiles of the measured data. The strongest absorbing
257 particles, Mesquite and Hickory, have *MAC* values about 5 times greater than that of the weakest
258 absorbers, Oak and Western redcedar. The *MAC* and *AAE* values of the 6 wood species measured
259 compare well to the suggested values by Reid, et al. (2005)⁴⁶ who conducted an extensive review
260 of smoldering forest fire data and concluded that the *MAC* of particles emitted during smoldering
261 are < 0.3 m² g⁻¹ at $\lambda = 550$ nm; these data suggest that a generalized wood-type independent value
262 for smoldering *MAC* of < 0.1 m² g⁻¹ may be more accurate. Previously, Chakrabarty, et al. (2016)¹⁹
263 measured a *MAC* of 3 x 10⁻² m² g⁻¹ to 7 x 10⁻² m² g⁻¹ at $\lambda = 532$ nm for smoldering peat samples
264 (50% moisture content) while Hoffer, et al. (2006)¹⁴ measured *MAC* of 2.9 x 10⁻² m² g⁻¹ to 3.1 x
265 10⁻² m² g⁻¹ at $\lambda = 532$ nm for fine-fraction isolates of Amazon basin biomass-burning aerosol. Both
266 of these previous values compare well to the results reported in this study.

267 **BC Contribution.** Following the convention used in other investigations, it can be assumed that
268 BrC does not absorb significantly in the in near-IR spectral region ($\lambda = 840$ nm) and that all
269 absorption at 840 nm corresponds to BC. Using this assumption, the estimated BC contribution is
270 a maximum of 0.4 % by mass (Mesquite, see Table 1), but is likely closer to 0.1 % by mass by
271 taking into account refractive index matching^{47,48} (see Supporting Information). If present, the BC
272 per particle is below the detection limit of even the most sensitive current *in-situ* BC techniques,
273 consistent with the lack of observed BC in the presented SWP TEM images. Subtracting the noted
274 BC spectral contribution increased the calculated AAE to between 7.0 and 35 (see Table 1) similar
275 to results from smoldering peat using the same fitting routine.⁴

276 **DISCUSSION**

277 The present data, to our knowledge, represent the first direct, *in-situ* MAC spectra of SWP. MAC
278 is directly calculated from three measured quantities (absorption coefficients, mass and number
279 density) that, more importantly, do not require any assumptions of particle chemical composition,
280 material density or morphology as is required for filter-based solvent-extraction or compositional
281 analysis measurements. In this investigation, the instrumental calibration uncertainties are on the
282 order of few percent (see Supporting Information). As a result, unlike these other methods, the
283 MAC and wavelength dependencies are dominated by the variability in particle absorption (Type
284 A uncertainty) allowing for quantitative comparison between spectra.

285 Using the Wilcox rank-sum test, point-by-point comparison of the individual SWP absorption
286 spectra reveals that Oak, Western redcedar and Blue spruce are statistically similar ($p > 0.05$) while
287 Hickory, Mesquite and Baldcypress were each distinct ($p < 0.01$); see Supporting Information for
288 analysis statistics. The data suggest that, for smoldering biomass, MAC and spectral shape can be
289 species dependent.

290 The measured absorption spectra are likely influenced by wood composition. Wood is composed
291 of lignin, cellulose, hemicellulose (HC), and extractives. Lignin is a phenolic biopolymer residing
292 between wood cell walls that thermally degrades slowly between 225 °C and 700 °C.^{33,49} Cellulose
293 forms the fibrous tissue in wood and is composed of up to 10^3 glucose units arranged in a
294 multilayered, hydrogen bonded structure that make it thermally stable up to 800 °C.³³ HC
295 comprises wood cell walls that accounts for up to 50 % of wood's mass. Nearly 90 % of the HC
296 in deciduous trees (encompassing most hardwood species) are xylans, a family of xylose
297 polysaccharides, that thermally degrade between 200 °C and 300 °C.³³ Softwood species HC is
298 additionally composed of glucomannan (a branched polysaccharide) and arabinogalactan (an
299 arabinose and galactose monosaccharide), both of which thermally degrade over the same
300 temperature range as xylans. Extractives are non-structural constituents that are chemically distinct
301 for each wood specie that account for \approx 1% by mass. Unlike structural components, the
302 composition and mass percentage of extractives may vary greatly in different parts of biomass
303 (wood, bark, needles, leaves). Hardwood extractives consist of fatty acids and phenolic compounds
304 (stilbenes, lignans, etc) while softwood extractives are mostly resins of terpenes and terpene
305 derivatives.³³

306 Thermocouple readings taken within the smoldering chamber were < 280 °C, below the flaming
307 initiation temperature for hardwoods (300 °C) and softwoods (350 °C), minimizing BC
308 formation.⁵⁰ Thermal decomposition via smoldering is initiated by xylose thermolysis, forming
309 and releasing acetic and formic acids. Both acids catalyze HC thermal decomposition releasing a
310 mixture of gaseous products and condensable species.⁵¹ The products formed from HC and
311 extractive thermal degradation and release have been shown to be chemically distinct for each
312 wood specie. For example, the condensed phase emissions of Scots pine (*pinus sylvestris*) heated

313 between 200 °C and 260 °C measured 21% H₂O, 8% acetic acid, 5% formic acid, nearly 4 %
314 methanol and the balance was a mixture of organic species.⁵² Smoldering Northern spruce (*picea*
315 *abies*) thermal decomposition products were 90% acetic and formic acids by mass with a few
316 percent each of fatty acids, resins and phenolic compounds.⁵³ Lastly, studies that heated a range of
317 biomass types between 250 °C and 300 °C collected light brown, viscous tar-like products,
318 consistent with the presented TEM images and spectroscopic measurements.⁵²

319 Previous studies of BB have been divided whether fuel type or combustion conditions have the
320 largest influence on particle optical properties. Correlations of the light absorbing carbon contained
321 in aerosol and the calculated imaginary refractive index have been demonstrated,²² while other
322 studies suggest that particle absorption is independent of biomass fuel type but dependent on burn
323 conditions (ratio of smoldering to flaming combustion).³¹ The data reported in this investigation
324 of particles produced from controlled low temperature smoldering indicates that both *MAC* and
325 *AAE* can be influenced by fuel type. Measured particle absorption spectra from six wood species
326 showed that the SWP *MAC* and spectral shape of three species were statistically distinct while
327 three were statistically similar. The six wood species had measured median *MAC* values spanning
328 between 0.014 m² g⁻¹ and 0.079 m² g⁻¹ at $\lambda = 550$ nm and *AAEs* ranging from 3.5 (Mesquite) to 6.2
329 (Blue spruce).

330 **ASSOCIATED CONTENT**

331 **Supporting Information.** Contains additional TEM images of Oak and Blue spruce particles.
332 Description of the data analysis procedure and Oak SWP smoldering stability is presented.
333 Calculations of Oak refractive index at $\lambda = 660$ nm from C_{abs} data is presented. Refractive index is
334 then extended to $\lambda = 500$ nm and 840 nm to demonstrate *MAC* mass independence over the range
335 of particle sizes measured. Details on the calculation of BC mass fraction and instrumental

336 uncertainties are presented. Finally, spectral correlation tables for the Wilcoxon Rank-sum
337 calculations are included. Supporting Information is available free of charge on the ACS
338 Publications website.

339 **AUTHOR INFORMATION**

340 **Corresponding Author**

341 * E-mail: cdzang@nist.gov. Phone: (301)975-8709. Fax: (301)975-3670

342 **Author Contributions**

343 The manuscript was written through contributions of all authors. All authors have given approval
344 of the final version of the manuscript.

345 **Notes**

346 The authors declare no competing financial interests.

347

348 **REFERENCES**

349 (1) IPCC, Changes in Atmospheric Constituents and in Radiative Forcing. In *Contribution of*
350 *Working Group I to the Fourth Assessment Report of the Intergovernmental Panel on Climate*
351 *Change, 2007*, Solomon, S.; Qin, D.; Manning, M.; Chen, Z.; Marquis, M.; Averyt, K. B.; Tignor,
352 M.; Miller, H. L., Eds. Cambridge University Press: Cambridge, United Kingdom and New York,
353 NY, USA, 2007; pp 129–234.

354 (2) Pöschl, U., Atmospheric aerosols: Composition, transformation, climate and health effects.
355 *Angew. Chem., Int. Ed.* **2005**, *44* (46), 7520-7540.

356 (3) Martinsson, J.; Eriksson, A. C.; Nielsen, I. E.; Malmberg, V. B.; Ahlberg, E.; Andersen,
357 C.; Lindgren, R.; Nyström, R.; Nordin, E. Z.; Brune, W. H.; Svenningsson, B.; Swietlicki, E.;
358 Boman, C.; Pagels, J. H., Impacts of combustion conditions and photochemical processing on the
359 light absorption of biomass combustion aerosol. *Environ. Sci. Technol.* **2015**, *49* (24), 14663-
360 14671.

361 (4) Chakrabarty, R. K.; Moosmuller, H.; Chen, L. W. A.; Lewis, K.; Arnott, W. P.; Mazzoleni,
362 C.; Dubey, M. K.; Wold, C. E.; Hao, W. M.; Kreidenweis, S. M., Brown carbon in tar balls from
363 smoldering biomass combustion. *Atmos. Chem. Phys.* **2010**, *10* (13), 6363-6370.

364 (5) Sato, M.; Hansen, J.; Koch, D.; Lacis, A.; Ruedy, R.; Dubovik, O.; Holben, B.; Chin, M.;
365 Novakov, T., Global atmospheric black carbon inferred from AERONET. *Proc. Natl. Acad. Sci.*
366 *U. S. A.* **2003**, *100* (11), 6319-6324.

367 (6) Bond, T. C.; Doherty, S. J.; Fahey, D. W.; Forster, P. M.; Berntsen, T.; DeAngelo, B. J.;
368 Flanner, M. G.; Ghan, S.; Kärcher, B.; Koch, D.; Kinne, S.; Kondo, Y.; Quinn, P. K.; Sarofim, M.
369 C.; Schultz, M. G.; Schulz, M.; Venkataraman, C.; Zhang, H.; Zhang, S.; Bellouin, N.; Guttikunda,
370 S. K.; Hopke, P. K.; Jacobson, M. Z.; Kaiser, J. W.; Klimont, Z.; Lohmann, U.; Schwarz, J. P.;
371 Shindell, D.; Storelvmo, T.; Warren, S. G.; Zender, C. S., Bounding the role of black carbon in the
372 climate system: A scientific assessment. *J. Geophys. Res.: Atmos.* **2013**, *118*, 5380 - 5552.

373 (7) Bond, T. C.; Bergstrom, R. W., Light absorption by carbonaceous particles: An
374 investigative review. *Aerosol Sci. Tech.* **2006**, *40* (1), 27-67.

375 (8) Andreae, M. O.; Gelencser, A., Black carbon or brown carbon? The nature of light-
376 absorbing carbonaceous aerosols. *Atmos. Chem. Phys.* **2006**, *6* (10), 3131-3148.

377 (9) IPCC, *Climate Change 2013: The Physical Science Basis. Contribution of Working Group*
378 *I to the Fifth Assessment Report of the Intergovernmental Panel on Climate Change*. Cambridge
379 University Press: Cambridge, United Kingdom and New York, NY, USA, 2013; p 1535.

380 (10) Jacobson, M. Z., Effects of biomass burning on climate, accounting for heat and moisture
381 fluxes, black and brown carbon, and cloud absorption effects. *J. Geophys. Res.: Atmos.* **2014**, *119*
382 (14), 8980-9002.

383 (11) Feng, Y.; Ramanathan, V.; Kotamarthi, V. R., Brown carbon: a significant atmospheric
384 absorber of solar radiation? *Atmos. Chem. Phys.* **2013**, *13* (17), 8607-8621.

385 (12) Ångström, A., On the atmospheric transmission of sun radiation and on dust in the air.
386 *Geogr. Ann.* **1929**, *11*, 156 - 166.

387 (13) Moosmüller, H.; Chakrabarty, R. K.; Ehlers, K. M.; Arnott, W. P., Absorption Ångström
388 coefficient, brown carbon, and aerosols: basic concepts, bulk matter, and spherical particles.
389 *Atmos. Chem. Phys.* **2011**, *11* (3), 1217-1225.

390 (14) Hoffer, A.; Gelencsér, A.; Guyon, P.; Kiss, G.; Schmid, O.; Frank, G. P.; Artaxo, P.;
391 Andreae, M. O., Optical properties of humic-like substances (HULIS) in biomass-burning
392 aerosols. *Atmos. Chem. Phys.* **2006**, *6* (11), 3563-3570.

393 (15) O'Neill, N. T.; Eck, T. F.; Holben, B. N.; Smirnov, A.; Royer, A.; Li, Z., Optical properties
394 of boreal forest fire smoke derived from Sun photometry. *J. Geophys. Res.: Atmos.* **2002**, *107*
395 (D11), AAC 6-1–AAC 6-19.

396 (16) Srinivas, B.; Rastogi, N.; Sarin, M. M.; Singh, A.; Singh, D., Mass absorption efficiency
397 of light absorbing organic aerosols from source region of paddy-residue burning emissions in the
398 Indo-Gangetic Plain. *Atmos. Environ.* **2016**, *125, Part B*, 360-370.

399 (17) Lee, S.; Baumann, K.; Schauer, J. J.; Sheesley, R. J.; Naeher, L. P.; Meinardi, S.; Blake,
400 D. R.; Edgerton, E. S.; Russell, A. G.; Clements, M., Gaseous and particulate emissions from
401 prescribed burning in Georgia. *Environ. Sci. Technol.* **2005**, *39* (23), 9049-9056.

402 (18) Holder, A. L.; Hagler, G. S. W.; Aurell, J.; Hays, M. D.; Gullett, B. K., Particulate matter
403 and black carbon optical properties and emission factors from prescribed fires in the southeastern
404 United States. *J. Geophys. Res.: Atmos.* **2016**, *121* (7), 3465-3483.

405 (19) Chakrabarty, R. K.; Gyawali, M.; Yatavelli, R. L. N.; Pandey, A.; Watts, A. C.; Knue, J.;
406 Chen, L. W. A.; Pattison, R. R.; Tsibart, A.; Samburova, V.; Moosmüller, H., Brown carbon
407 aerosols from burning of boreal peatlands: microphysical properties, emission factors, and
408 implications for direct radiative forcing. *Atmos. Chem. Phys.* **2016**, *16* (5), 3033-3040.

409 (20) Chen, L. W. A.; Moosmüller, H.; Arnott, W. P.; Chow, J. C.; Watson, J. G.; Susott, R. A.;
410 Babbitt, R. E.; Wold, C. E.; Lincoln, E. N.; Hao, W. M., Particle emissions from laboratory
411 combustion of wildland fuels: In situ optical and mass measurements. *Geophys. Res. Lett.* **2006**,
412 *33* (4), L04803.

413 (21) Chen, L. W. A.; Moosmüller, H.; Arnott, W. P.; Chow, J. C.; Watson, J. G.; Susott, R. A.;
414 Babbitt, R. E.; Wold, C. E.; Lincoln, E. N.; Hao, W. M., Emissions from laboratory combustion
415 of wildland fuels: Emission factors and source profiles. *Environ. Sci. Technol.* **2007**, *41* (12),
416 4317-4325.

417 (22) Levin, E. J. T.; McMeeking, G. R.; Carrico, C. M.; Mack, L. E.; Kreidenweis, S. M.;
418 Wold, C. E.; Moosmüller, H.; Arnott, W. P.; Hao, W. M.; Collett, J. L., Jr.; Malm, W. C., Biomass
419 burning smoke aerosol properties measured during Fire Laboratory at Missoula Experiments
420 (FLAME). *J. Geophys. Res.* **2010**, *115* (D18), D18210.

421 (23) Mack, L. A.; Levin, E. J. T.; Kreidenweis, S. M.; Obrist, D.; Moosmüller, H.; Lewis, K.
422 A.; Arnott, W. P.; McMeeking, G. R.; Sullivan, A. P.; Wold, C. E.; Hao, W. M.; Collett Jr, J. L.;

423 Malm, W. C., Optical closure experiments for biomass smoke aerosols. *Atmos. Chem. Phys.* **2010**,
424 *10* (18), 9017-9026.

425 (24) Pandey, A.; Pervez, S.; Chakrabarty, R. K., Filter-based measurements of UV–vis mass
426 absorption cross sections of organic carbon aerosol from residential biomass combustion:
427 Preliminary findings and sources of uncertainty. *J. Quant. Spectrosc. Radiat. Transfer* **2016**, *182*,
428 296-304.

429 (25) Hungershoefer, K.; Zeromskiene, K.; Iinuma, Y.; Helas, G.; Trentmann, J.; Trautmann,
430 T.; Parmar, R. S.; Wiedensohler, A.; Andreae, M. O.; Schmid, O., Modelling the optical properties
431 of fresh biomass burning aerosol produced in a smoke chamber: results from the EFEU campaign.
432 *Atmos. Chem. Phys.* **2008**, *8* (13), 3427-3439.

433 (26) Chen, Y.; Bond, T. C., Light absorption by organic carbon from wood combustion. *Atmos.*
434 *Chem. Phys.* **2010**, *10* (4), 1773-1787.

435 (27) Saleh, R.; Hennigan, C. J.; McMeeking, G. R.; Chuang, W. K.; Robinson, E. S.; Coe, H.;
436 Donahue, N. M.; Robinson, A. L., Absorptivity of brown carbon in fresh and photo-chemically
437 aged biomass-burning emissions. *Atmos. Chem. Phys.* **2013**, *13* (15), 7683-7693.

438 (28) Kirchstetter, T. W.; Novakov, T.; Hobbs, P. V., Evidence that the spectral dependence of
439 light absorption by aerosols is affected by organic carbon. *J. Geophys. Res.: Atmos.* **2004**, *109*,
440 D21208.

441 (29) Barnard, J. C.; Volkamer, R.; Kassianov, E. I., Estimation of the mass absorption cross
442 section of the organic carbon component of aerosols in the Mexico City Metropolitan Area. *Atmos.*
443 *Chem. Phys.* **2008**, *8* (22), 6665-6679.

444 (30) Ajtai, T.; Filep, Á.; Utry, N.; Schnaiter, M.; Linke, C.; Bozóki, Z.; Szabó, G.; Leisner, T.,
445 Inter-comparison of optical absorption coefficients of atmospheric aerosols determined by a multi-
446 wavelength photoacoustic spectrometer and an Aethalometer under sub-urban wintry conditions.
447 *J. Aerosol Sci.* **2011**, *42* (12), 859-866.

448 (31) Saleh, R.; Robinson, E. S.; Tkacik, D. S.; Ahern, A. T.; Liu, S.; Aiken, A. C.; Sullivan, R.
449 C.; Presto, A. A.; Dubey, M. K.; Yokelson, R. J.; Donahue, N. M.; Robinson, A. L., Brownness of
450 organics in aerosols from biomass burning linked to their black carbon content. *Nat. Geosci.* **2014**,
451 *7* (9), 647-650.

452 (32) Radney, J. G.; Ma, X.; Gillis, K. A.; Zachariah, M. R.; Hodges, J. T.; Zangmeister, C. D.,
453 Direct measurements of mass-specific optical cross sections of single component aerosol mixtures.
454 *Anal. Chem.* **2013**, *85* (17), 8319-8325.

455 (33) Tumuluru, J. S.; Sokhansanj, S.; Hess, J. R.; Wright, C. T.; Boardman, R. D., A review
456 on biomass torrefaction process and product properties for energy applications. *Ind. Biotechnol.*
457 **2011**, *7* (5), 384-401.

458 (34) Ohlemiller, T. J., Smoldering Combustion Propagation On Solid Wood. *Fire Saf. Sci.*
459 **1991**, *3*, 565-574.

460 (35) Radney, J. G.; Zangmeister, C. D., Practical limitations of aerosol separation by a tandem
461 differential mobility analyzer–aerosol particle mass analyzer. *Aerosol Sci. Tech.* **2016**, *50* (2), 160-
462 172.

463 (36) Park, K.; Cao, F.; Kittelson, D. B.; McMurry, P. H., Relationship between particle mass
464 and mobility for diesel exhaust particles. *Environ. Sci. Technol.* **2003**, *37* (3), 577-583.

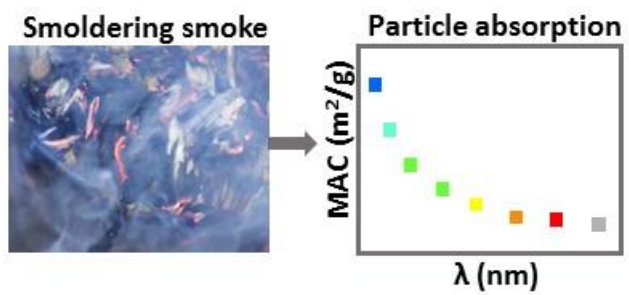
465 (37) McMurry, P. H.; Wang, X.; Park, K.; Ehara, K., The relationship between mass and
466 mobility for atmospheric particles: A new technique for measuring particle density. *Aerosol Sci.*
467 *Tech.* **2002**, *36* (2), 227-238.

- 468 (38) Radney, J. G., Zangmeister, C. D., Measurement of gas and aerosol phase absorption
469 spectra across the Visible and near-IR using Supercontinuum photoacoustic spectroscopy. *Anal.*
470 *Chem.* **2015**, *87*, 7356-7363.
- 471 (39) Reid, J. S.; Koppmann, R.; Eck, T. F.; Eleuterio, D. P., A review of biomass burning
472 emissions part II: intensive physical properties of biomass burning particles. *Atmos. Chem. Phys.*
473 **2005**, *5* (3), 799-825.
- 474 (40) Buseck, P. R.; Adachi, K.; Andras, G.; Tompa, E.; Mihaly, P., Ns-Soot: A material-based
475 term for strongly light-absorbing carbonaceous particles. *Aerosol Sci. Tech.* **2014**, *48* (7), 777-788.
- 476 (41) Subramanian, R.; Roden, C. A.; Boparai, P.; Bond, T. C., Yellow beads and missing
477 particles: Trouble ahead for filter-based absorption measurements. *Aerosol Sci. Tech.* **2007**, *41* (6),
478 630-637.
- 479 (42) Sun, H.; Biedermann, L.; Bond, T. C., Color of brown carbon: A model for ultraviolet and
480 visible light absorption by organic carbon aerosol. *Geophys. Res. Lett.* **2007**, *34*, L17813.
- 481 (43) Hijmans, R. GADM Database of Global Administrative Areas. <http://gadm.org> (July 27,
482 2016)
- 483 (44) U. S. Geological Survey, Digital representation of "Atlas of United States Trees" by Elbert
484 L. Little, Jr. <http://gec.cr.usgs.gov/data/little> (July 27, 2016).
- 485 (45) You, R.; Radney, J. G.; Zachariah, M. R.; Zangmeister, C. D., Measured wavelength-
486 dependent absorption enhancement of internally mixed black carbon with absorbing and
487 nonabsorbing materials. *Environ. Sci. Technol.* **2016**, *50* (15), 7982-7990.
- 488 (46) Reid, J. S.; Eck, T. F.; Christopher, S. A.; Koppmann, R.; Dubovik, O.; Eleuterio, D. P.;
489 Holben, B. N.; Reid, E. A.; Zhang, J., A review of biomass burning emissions part III: intensive
490 optical properties of biomass burning particles. *Atmos. Chem. Phys.* **2005**, *5* (3), 827-849.
- 491 (47) Jacobson, M. Z., A physically-based treatment of elemental carbon optics: Implications
492 for global direct forcing of aerosols. *Geophys. Res. Lett.* **2000**, *27* (2), 217-220.
- 493 (48) Yablonoitch, E., Statistical ray optics. *J. Opt. Soc. Am.* **1982**, *72* (7), 899-907.
- 494 (49) Yang, H.; Yan, R.; Chen, H.; Lee, D. H.; Zheng, C., Characteristics of hemicellulose,
495 cellulose and lignin pyrolysis. *Fuel* **2007**, *86* (12-13), 1781-1788.
- 496 (50) Babrauskas, V., *Ignition of Wood: A Review of the State of the Art*, Interflam 2001,
497 London, 2001; Interscience Communications Limited: London, 2001; pp 71-88.
- 498 (51) Bourgois, J.; Guyonnet, R., Characterization and analysis of torrefied wood. *Wood Sci.*
499 *Technol.* **1988**, *22* (2), 143-155.
- 500 (52) Esteves, B. M.; Pereira, H. M., Wood modification by heat treatment: A review.
501 *BioResources* **2009**, *4* (1), 370-404.
- 502 (53) Alen, R.; Kotilainen, R.; Zaman, A., Thermochemical behavior of Norway spruce (*Picea*
503 *abies*) at 180-225 degrees C. *Wood Sci. Technol.* **2002**, *36* (2), 163-171.

504

505

506 TOC FIGURE



507

508

509